Polymer Bulletin (2024) 81:11007–11026
https://doi.org/10.1007/s00289-024-05225-w

ORIGINAL PAPER

Effect of different compatibilization routes on the mechanical, thermal and rheological properties of polypropylene/cellulose nanocrystals nanocomposites

Lilia Benchikh[1] · Tahar Aouissi[2] · Yazid Aitferhat[3] · Hichem Chorfi[3] · Ilyes Abacha[3] · Maya Kebaili[3] · Melia Guessoum[4] · Abdelhafid Merzouki[4] · Yves Grohens[5] · Mauro Carraro[6,7] · Souad Djellali[4,8]

Received: 27 September 2023 / Revised: 19 February 2024 / Accepted: 22 February 2024 /
Published online: 21 March 2024

Abstract

The combination of cellulose nanocrystals (CNCs) with synthetic polymers like polypropylene (PP) offers the opportunity to create advanced nanocomposites with significant advantages in terms of mechanical properties, improved thermal stability, enhanced barrier properties, and sustainability. However, a major drawback for incorporation of CNCs in polymer matrices is their poor dispersion and incompatibility with industrial processing of many composites. This work aims to improve the dispersion of hydrophilic CNCs in a hydrophobic matrix using a method which could be adapted for the industrial level. CNCs are extracted from *Ampelodesmos mauritanicus* (El Diss plant) (CNC_D) and incorporated in a polypropylene matrix using the masterbatch method. A first nanocomposite (PP/CNC-Gr) was prepared by adding maleic anhydride (MA) to a CNC_D/PP suspension, while the second nanocomposite (PP/CNC-Co) was achieved by using a MA-grafted PP (PP-g-MA) as a third component. Concentrated masterbatch underwent solution casting followed by homogenization in a Brabender mixer. Mechanical properties comparison showed that PP/CNC-Co nanocomposites exhibited greater resistance relatively to PP/CNC-Gr nanocomposites. Moreover, PP/CNC-Co nanocomposites revealed an improved thermal stability and a higher complex viscosity, particularly with 3% of CNC_D. Properties enhancements are attributed to the reaction between MA groups grafted to PP chains and hydroxyl groups of CNC_Ds, which enables an improved interfacial adhesion, leading to more continuous materials, as perceived from the increase in viscosity and morphology observation. On the other hand, MA reaction with PP chains and CNC_D induced only a partial coverage of CNC_Ds during nanocrystals treatment, conferring relatively lower properties to PP/CNC-Gr nanocomposites.

Extended author information available on the last page of the article

Keywords Cellulose nanocrystals · Compatibilization · Masterbatch · Nanocomposites · Maleic anhydride

Introduction

Apprehensions about global warming, energy security and the continuous depleting of fossil reserves are disquieting both academicians and industrialists [1]. As a consequence, businesses and governments are basing their strategies towards sustainable development on the encouragement of gradual shift from the traditional hydrocarbon-based "oil refinery" to the sustainable biomass-based "biorefinery", as a vital priority [2, 3]. Accordingly, polymeric materials from renewable natural sources and natural fiber-reinforced composites are attracting increasing attention for their lower environmental impact [4, 5]. However, to replace petroleum-based thermoplastics, biopolymers need to have comparable properties and processing methods to those commonly used. Alternatively, fibers derived from natural resources can be incorporated into conventional and biosourced polymers to obtain more ecofriendly materials [6].

Due to their reduced size and good dispersion into the polymer matrix, nanomaterials-based composites exhibit markedly improved properties when compared to the pure (synthetic or natural) polymers [5]. Consequently, an explosive growth of nanotechnology has fueled hectic research on lignocellulosic materials, whose use has almost veered from micro- to nanoscale [7]. Cellulosic nanocrystals (CNCs), in particular, are preferred as load-bearing constituents, due to their greater ability to improve toughness along with strength and stiffness through CNCs-matrix interface interactions [8].

Cellulosic fibers are a nearly inexhaustible, cheap and readily available raw material, conferring an endless source for low cost CNC's production [9]. The nanocellulosic structure can be extracted from plants by a top-down approach into well-defined and multi-functional architectures. One of the most used methods for CNCs extraction from pure cellulose fibers is the complete degradation and dissolution of noncrystalline parts by hydrolysis reactions [10, 11].

As the size of a particle is decreasing down to the nanometer scale, important changes occur. For example, a spherical particle on a nanometer scale diameter can have about 50% of its atoms on the surface. As consequence, both the specific surface area and total surface energy of the nanoparticles increase, resulting in a stronger tendency to form agglomerates. This issue is particularly significant for cellulose, which displays a reactive surface, with plenty of hydroxyl groups [12, 13]. Moreover, the poor adhesion at the interface between hydrophobic polymer matrices and extremely hydrophilic CNCs, due to the absence of sufficient and adequate interactions, induces properties deterioration, making the ensuing composite unusable [14, 15].

Within this scenario, it was reported that the concentration and dispersion quality of nanocellulose in polypropylene (PP) and polyethylene (PE) matrices play a crucial role on the mechanical behavior and environment-friendly character of the developed nanocomposites. Polyolefin/CNC nanocomposites can also lead to lighter

materials with comparable or even superior performance to traditional plastics. This reduction in weight, in turn, can contribute to energy savings and reduce transportation costs.

The adhesion enhancement can be ensured by fibers surface modification, exploiting the abundant hydroxyl groups at CNCs surface, and resulting in the promotion of interactions via compatibilization, coupling, acetylation or polymer grafting processes, among many other available treatment methods [16–18].

Maleated coupling agents have been widely applied to nanocellulose-reinforced composites and proved their efficiency in improving interfacial bonding between CNCs and polymers by ensuring a uniform nanocrystals dispersion into the matrix [9, 19]. Besides, solvent exchange, i.e., the replacement of water in CNC suspension with other organic solvents during CNC's chemical modification, was reported as a suitable route to increase the overall processability and reduce lateral agglomeration [16].

Different processing techniques for nanocellulose-based nanocomposites have been described, including solution-casting, melt-extrusion, electrospinning, etc., whereby the first one is among the most suitable methods to obtain a good dispersion of nanocellulose within the polymer solution [20]. However, in industry, the preferential way to obtain CNC reinforced nanocomposites is the melting mixing process, feeding dried CNC instead of using laboratory scale solution-casting of polymer with suspended CNCs, even if CNC agglomeration increases with the dry process. On the other hand, feeding a water suspension of CNC into the extruder during the melt processing has been found to be challenging for the risk of foaming during water evaporation [5, 21].

This work aims to, firstly, attest the effectiveness of maleic anhydride as a compatibilizer for obtaining a CNC_D optimal dispersion when it is directly chemically grafted to PP in the CNC_D suspension for the nanocomposites noted PP/CNC-Gr or incorporated into the PP mixture/CNC_D through a commercial compatibilizer, therefore grafted beforehand to get the nanocomposites noted PP/CNC-Co. The second goal of the study is to verify the usefulness of the procedure consisting of using the masterbatch method, like the solution casting method, to achieve better dispersion, then carrying out melt mixing to veer to the industrial routes. The obtained nanocomposite materials were characterized by different thermal, mechanical and rheological techniques. CNC_D's dispersion state in the PP matrix was also monitored by electron microscopy.

Materials and methods

CNCs were extracted from El Diss (*Ampelodesmos mauritanicus*), which is a local and abundant plant in the region of Sétif (Algeria). CNC_D nanocrystals preparation method and characterization details were reported earlier by Benchikh and al. [22]. The used polypropylene is "HG385MO" produced by "Borouge", with a density of 0.91 g/cm^3 and a melt flow index of 25 g/10 min (at 230 °C and under 2.16 kg). The reagents used for CNC_D modification were: sodium hydroxide (NaOH), maleic anhydride ($C_4H_2O_3$) and xylene (C_8H_{10}) purchased from Sigma Aldrich (St. Louis,

Missouri, United States). Acetone (C_3H_6O), methanol (CH_3OH) and ethanol (CH_3CH_2OH) are from Biochem Chemical Pharma (Montreal, Quebec, Canada). Dicumyl peroxide (DCP) is supplied by Acros (Belgium) and its decomposition temperature is 140 °C.

CNC_D modification

CNC_D desulfation

This step was followed in order to eliminate sulfate groups from CNC_D surface, resulting from hydrolysis acid with sulfuric acid, to ensure better dispersion in organic solvents.

CNC_D suspension obtained after centrifugation was dispersed in distilled water and placed in an ultrasonic bath for 10 min. Then, NaOH solution (1% wt) was added, and the mixture was stirred at 60 °C for 3 h. Afterwards, CNC_D were washed with distilled water by centrifugation at 4000 rpm for 15 min.

Solvent exchange for CNC_D suspension

The dispersion of desulfated CNC_D in xylene was carried out by solvent exchange method. After CNC_D precipitation by centrifugation and water removal, ethanol was added. The obtained suspension was subjected to ultrasounds for 10 min, and then centrifuged again at 4000 rpm for 20 min to remove the solvent (this step is repeated 3 times). The same operation was repeated with acetone, methanol and finally with xylene.

Preparation of CNC-Gr

After introducing a suspension of 4 g of CNC_D in 15 mL of xylene into an ultrasonic bath for 30 min, it was brought to 140 °C by a hot oil bath and 1 g of PP was added. Once PP granules were completely dissolved (40 min), 0.2 g of MA and 0.002 g of DCP were added to the PP/CNC_D suspension and the reaction was kept for 2 h. Finally, the obtained CNC-Gr mixture was washed by centrifugation and then dried. CNC_D reaction with maleic anhydride is reported in Fig. 1.

Formulation of PP/CNC_D nanocomposites

Masterbatches preparation

Two types of masterbatches were prepared, one from unmodified CNC_D and the other with CNC-Gr, as shown in Fig. 2. After redispersion of CNC_D/xylene suspension and CNC-Gr in xylene and treating by sonication for 10 min, PP was added to the CNC_D and CNC-Gr suspensions (with a ratio 1:4 w/w). In parallel, commercial PP-g-MA was incorporated to the non-grafted CNC_D suspension and the whole was placed under mechanical stirring (Heidolph RZR 2041) at 140 °C until complete

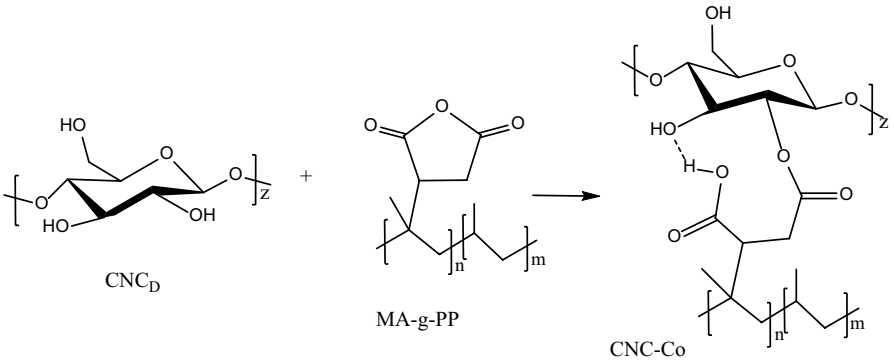

Fig. 1 CNC$_D$ reaction with PP-g-MA

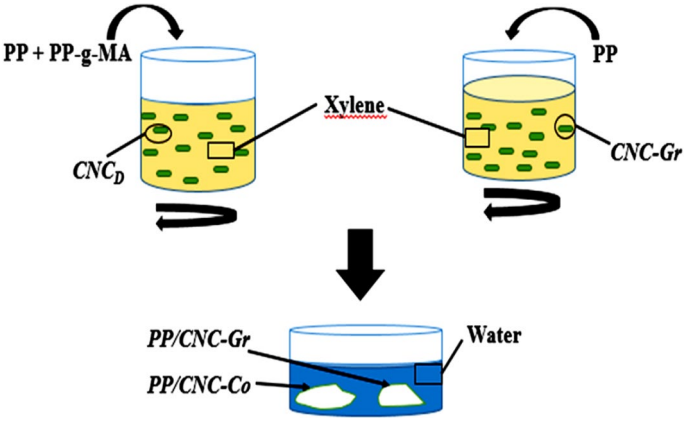

Fig. 2 Masterbatch preparation scheme

dissolution of PP and PP-g-MA. CNC$_D$ composition ratio to PP matrix is 5% wt and PP-g-MA to PP was 80/20 (w/w). After PP/CNC-Co and PP/CNC-Gr homogenization, the mixtures were immersed in distilled water to recover solid masterbatches, which were finally dried at 60 °C for 24 h.

Nanocomposites preparation

The PP composites obtained from the previously prepared masterbatches were melt-mixed in a Brabender plastograph at 190 °C, at a mixing speed of 50 rpm for 8 min. The formulations names assigned according to the CNC$_D$ content and type are shown in Table 1.

The obtained formulations were compressed into test samples using a Carver™ hydraulic press (Hampton, New Hampshire, USA). Compression molding was carried out according to the following conditions: Plate's temperature: 190 °C,

Table 1 Composition of PP/CNC-Gr and PP/CNC-Co nanocomposites

Formulations	CNC_D (%)	CNC-Gr (%)	PP (%)
PP	–	–	100
PP/CNC-Co 1%	1	–	99
PP/CNC-Co 3%	3	–	97
PP/CNC-Co 5%	5	–	95
PP/CNC-Gr 1%	–	1	99
PP/CNC-Gr 3%	–	3	97
PP/CNC-Gr 5%	–	5	95

preheating: t = 10 min, compression, preheating: t = 5 min, degassing 5 times, compression, t = 5 min, cooling to open air: t = 3 min.

Characterization

Fourier transform infrared (FTIR) spectroscopy

To investigate, structural changes after adding modified and unmodified CNC_D particles and PP-g-MA to PP, PP/CNC-Gr and PP/CNC-Co nanocomposites were investigated by FTIR spectroscopy. The samples were analyzed using a Vertex 70 v FTIR spectrometer, in transmittance mode, in the range between 4000 cm^{-1} and 400 cm^{-1} at a nominal resolution of 4 cm^{-1}.

Mechanical tests

Tensile properties were evaluated using MTS Landmark® (MTS Systems Corporation (USA)) universal testing machine. Specimens were prepared in dumbbell shape according to ASTM-D 638 and tested at a drawing speed of 5 mm/min. Izod impact strength of nanocomposites was measured by assessing samples of dimensions (62 × 13 × 3) mm^3 using a Ceast Resil Impact instrument equipped with a hammer of 1.8 kg delivering an impact energy of 7.5 kJ. Four replicates were tested for each formulation.

Scanning electron microscopy (SEM)

Surface morphology of neat PP and nanocomposite samples was analyzed by the observation of the impact test fractured surfaces using JSM-6460 apparatus (JEOL Inc., MA, USA). For improving the contrast, the specimens' surfaces were gold coated before observation.

Parallel-plate rheometery

An Anton Paar CTD 450 rheometer with parallel-plate oscillatory mode was used to analyze the rheological behavior of the studied formulations. A frequency

sweep was performed over a range from 0.01 to 100 Hz at a temperature of 195 °C. To determine the linear viscoelastic domain, frequency scans were carried out at a constant deformation of 0.1% for virgin PP and 1% for PP/CNC_D nanocomposites. In this domain, indeed, the material responds linearly to changes in stress or strain.

Thermogravimetric analysis (TGA)

Thermal stability of PP/CNC-Co and PP/CNC-Gr nanocomposites was investigated using a Mettler Toledo TGA/DSC thermogravimetric analyzer. The samples aliquots (7–10 mg) were heated from 20 to 800 °C at a constant heating rate of 20 °C/min under nitrogen atmosphere.

Results and discussion

Structural characterization

Figure 3 displays FTIR spectra of PP, PP-g-MA and PP/CNC nanocomposites to highlight the reaction between CNC's surface and maleic anhydride grafted on PP, as shown in Fig. 2.

The chemical changes in the CNC's reaction with maleic anhydride are represented by considering the band of carbonyl (1630 cm^{-1}) and anhydride groups (1780 and 1860 cm^{-1}) [23]. Samyn [24], in the preparation of the plasma-polymerized films (MA-CNC), observed that the maleic anhydride cyclic ring structures have partially disappeared, through a shift in characteristic peaks towards 1781 cm^{-1} (ester) and 1735 cm^{-1} (carbonyl) indicating the esterification between the maleic anhydride and CNC surface during plasma polymerization of the nanocomposite films.

After CNC_D incorporation, FTIR spectra present no obvious changes, indicating that the matrix structure has not been affected or modified with new functional groups. It seems that the mass reaction and structural changes occurring at the interfacial region between the CNC_Ds and the matrix are too weak to be detected by FTIR [25]. However, some bands intensity increase for both nanocomposites, undoubtedly due to CNC's homogeneous dispersion within the matrix [26–28]. Moreover, two bands at 1060 cm^{-1} and 1165 cm^{-1} can be ascribed to the C–OH stretching vibrations of the alcohol groups and to the asymmetric stretching of the C–O–C group of the glucose ring of the cellulose [29, 30]. The intensity of the band observed at 3500 cm^{-1}, assigned to O–H bonds involved in intermolecular hydrogen bonds, is slightly decreased for the nanocomposites. This indicates that some hydroxyl groups reacted with the compatibilizer's anhydride groups. Two additional bands at 993 cm^{-1} and 849 cm^{-1} may belong to maleic anhydride and could correspond to C–O–C bonds stretching of the cyclic ether [31].

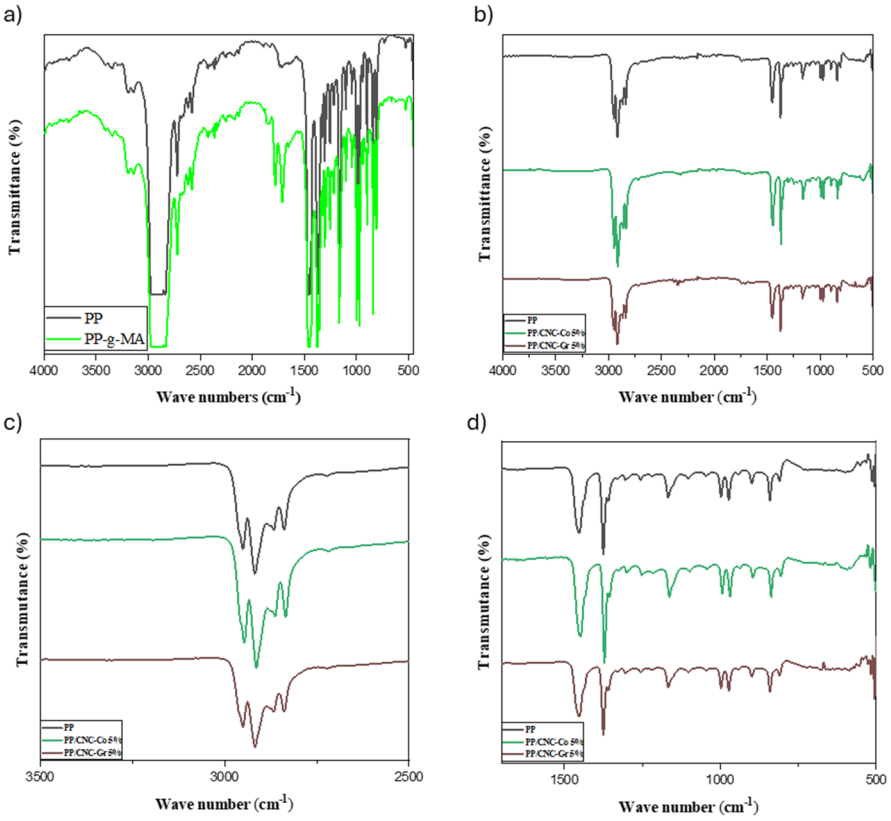

Fig. 3 **a** FTIR spectra of PP, PP-g-MA; **b** FTIR spectra of PP and nanocomposites, with enlarged regions (**c** and **d**)

Mechanical properties and morphology

To get insight into the quality of dispersion of CNCs nanoparticles and confirm the occurrence of interactions between CNC_Ds and PP matrix, mechanical tests and morphology observation seem to be the more adequate route. As it is shown from Fig. 4, giving the variations of impact strength for both types of PP/CNC_D nanocomposites versus CNC_D content, PP/CNC-Co nanocomposites have resilience values obviously higher than those of PP/CNC-Gr nanocomposites. Indeed, we observe a sensitive decrease in resilience from a value of 22 to 11 kJ/m^2 after adding only 1% of CNC-Gr. When increasing the CNC-Gr content up to 3%, the material resilience attains 14 kJ/m^2 then it decreases again notably for 5% PP/CNC-Gr nanocomposite, which displays a resilience of about 6 kJ/m^2. At 5%, the impact resistance decreases abruptly, thus pointing out the possibility of CNC_D agglomeration due to nanoparticles mutual interactions, generating structural defects within the matrix. The higher resilience values for PP/CNC-Co nanocomposites corroborate a much better stress transfer thanks to the interfacial reaction between CNC_D's hydroxyls and maleic

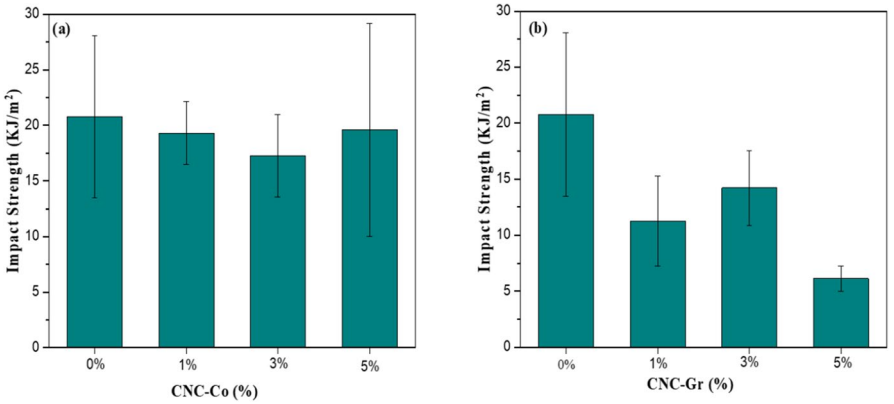

Fig. 4 Variations of impact strength for PP/CNC-Co (**a**) and PP/CNC-Gr (**b**) nanocomposites versus CNC_D content

anhydride groups available on PP-g-MA from one side and the entanglements of matrix's PP chains and PP-g-MA, from the other side. The synthesis of maleic anhydride-grafted PP in CNC_D solution, should activate maleic anhydride involving CNC_D surface esterification, where an absorption band, assigned to C=O symmetric stretching, appeared at 1714 cm^{-1} [32, 33]. Thus, despite CNC_D treatment with MA and their somewhat enrobing with PP chains were supposed to attenuate the hydrophilic character and induce a more intimate of CNC_D contact with the matrix, this strategy resulted in a poor adhesion, deteriorating the nanocomposites properties. In this context, Pinheiro et al. [34] observed that the mechanical properties of composites loaded with CNCs worsen when their content exceeds the percolation value, for which the dispersion is optimal. Also, it was stated that, in an optimal distribution, particles are prone to act as impact modifier for a polymer matrix [35]. Similarly, Garcia et al. [36] reported that in nanocomposites subjected to impact solicitation, interfacial regions are capable of resisting to cracks propagation more than the polymer matrix alone and this results from a distribution that is ideal, comparable to an impact modifier distribution. Moreover, Gwon et al. [33] reported improved tensile properties for nanocomposites obtained by solution pre-treatment before melt mixing into the extruder, compared to those directly extruded. They indicated, indeed, that maleic anhydride-modified CNCs disperse better in nanocomposites after solution pre-treatment, which argues the masterbatch method used in our study.

Stress-strain curves of PP/CNC-Co and PP/CNC-Gr nanocomposites are shown in Fig. 5. Also, Table 2 illustrates the tensile strength evolution, Young's modulus and the breaking strain evolution versus CNC_D content. At first view, tensile properties seem to fit well with the impact resistance results, in the sense that the PP/CNC-Co nanocomposites exhibit a more ductile behavior than that of PP/CNC-Gr ones. It is observed that PP/CNC-Co nanocomposites show higher tensile strength, modulus and strain values relatively to neat PP and PP/CNC-Gr. Such behavior confirms that PP-g-MA contributed in developing an effective interconnected structure relating PP matrix and CNC_Ds through the reaction of MA groups with the CNC_D's hydroxyls

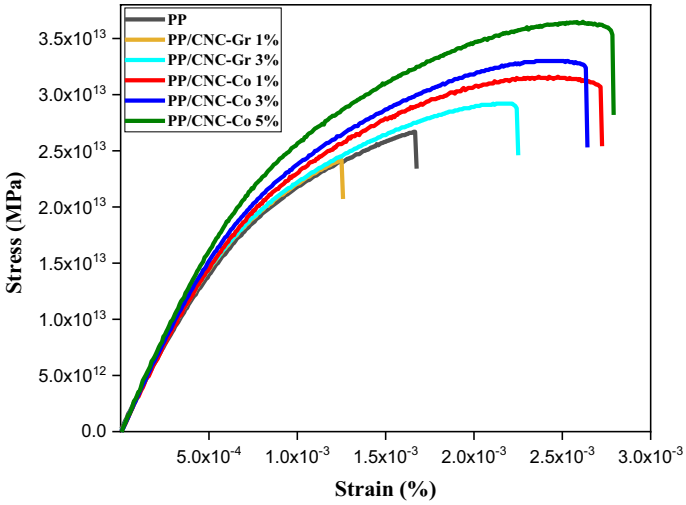

Fig. 5 Stress-strain curves of PP/CNC-Co and PP/CNC-Gr nanocomposites

Table 2 Tensile properties of PP/CNC-Co and PP/CNC-Gr nanocomposites

Formulation	Tensile strength (MPa)	Young modulus (MPa)	Elongation at break (%)
PP	23.8 ± 6.7	1946 ± 66	3.26 ± 0.48
PP/CNC-Co 1%	31.7 ± 4.7	2421 ± 57	4.92 ± 0.22
PP/CNC-Co 3%	32.7 ± 5.0	2491 ± 26	4.88 ± 0.07
PP/CNC-Co 5%	33.3 ± 12.8	2474 ± 104	4.8 ± 0.2
PP/CNC-Gr 1%	24.3 ± 2.5	2071 ± 41	2.49 ± 0.23
PP/CNC-Gr 3%	25.4 ± 6.0	1957 ± 79	3.08 ± 0.84

and the anchoring of the compatibilizer PP chains into the PP phase [36]. As a consequence of the synergistic effect between the nanoparticle's good dispersion into the matrix and the rigid interface relating the two components, a more efficient stress transfer is achieved, which is responsible for upgrading PP/CNC-Co nanocomposites tensile performances. The literature reports that the improvement of uniaxial traction properties is commonly ascribed to the homogeneous distribution of the CNCs into the polymer and the bonding of both the nanofiller and the matrix to the compatibilizer via chemical reactions or physical interactions [27, 37]. Accordingly, beside the chemical interactions, involving the ester bonds between CNCs and maleic anhydride (Fig. 1), also physical interactions, including van der Waals interactions and chains tangling between the PP matrix and PP backbones in PP-g-MA [34, 38] contribute to provide a continuous structure. On the other hand, PP/CNC-Gr nanocomposites reveal lower tensile strength, modulus and strain values denoting a lack of interactions between the matrix and the modified CNC_Ds. The weak adhesion could result from the fact that MA grafting on CNC_Ds does not involve all the

outer hydroxyl groups and so it fails in covering all the nanoparticles surface and in altering their hydrophilic character. It ensures that the poor tensile properties of PP/CNC-Gr nanocomposites could result from the absence of an efficient stress transfer caused by the lack of affinity between the hydrophilic and hydrophobic CNC_Ds and PP, respectively.

In order to assess CNC-Co and CNC-Gr nanoparticles dispersion quality within PP matrix, the nanocomposites morphology has been observed for the sample with 5% of CNC_Ds and the micrographs are shown in Fig. 6.

The texture of the pure matrix fracture surface is highly rough, thus implying a ductile failure mode of the polymer (micrograph (a, a′)). As well, The fracture surface of PP/CNC-Co nanocomposite containing 5% of CNC_D (micrographs (b, b′)), reveals a rough aspect which highlights the effective role of the compatibilizer to the energy absorption though ensuring an effective stress transfer at the interface PP/CNC_D. Indeed, the mutual interactions involved between CNC_D's and the compatibilizer's functional groups allow chemical bonding in addition to entanglements from PP chains side. This contributes also in disrupting nanoparticles aggregates, thus avoiding the formation of defects within the matrix. These observations are also corroborated by the fracture surface roughness which shows concomitantly the deviation of the crack's paths thanks to CNC_Ds, thus enhancing the sample resistance, through new cracks initiation processes [39–43].

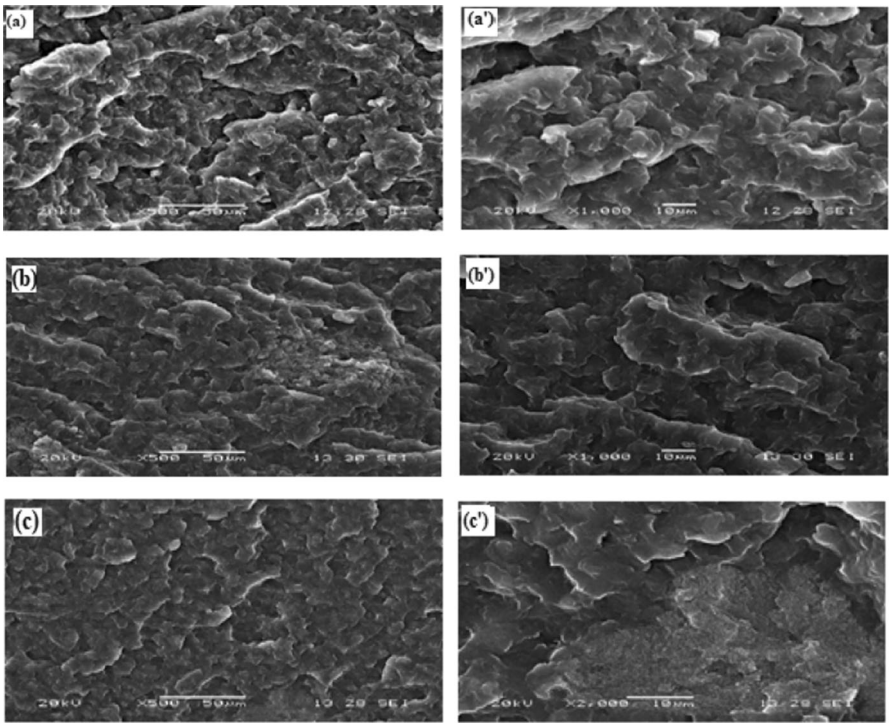

Fig. 6 SEM micrographs of PP/CNC_D nanocomposites: neat PP: (50 µm) (**a**) and 10 µm (**a′**), PP/CNC-Co 5%: (50 µm) (**b**) and 10 µm (**b′**) and PP/CNC-Gr 5%: (50 µm) (**c**) and 10 µm (**c′**)

Fig. 7 Variation of loss modulus G″ (**a**), storage modulus G′ (**b**) and complex viscosity (**c**) versus angular ▶ frequency for PP/CNC-Co and PP/CNC-Gr nanocomposites

However, as the CNC-Gr is incorporated (micrograph (c, c′)), the fracture surface becomes relatively smoother, thus pointing out a lower resistance during the material rupture. Due to the lack of affinity of the modified CNC_Ds for the hydrophobic matrix, particle/particle interactions are likely to be formed thus inducing a poor dispersion into the matrix [44]. As a result of the disadvantaged stress transfer in the interfacial region, a transition to more brittle fracture behavior, displaying limited energy dissipation, occurs as already pointed out by the mechanical tests [45].

Rheological characterization

To provide supplementary information regarding the dispersion state and mutual interactions relating CNC_D to the matrix in both sorts of nanocomposites, rheological measurements were carried out and the results, depicted as the variations of storage modulus (G′), loss modulus (G″) and complex viscosity (η*) versus frequency (Hz) are shown in Figs. 6c, 7a, b respectively.

At first sight, G′ and G″ of PP increase markedly in presence of CNC_D (Fig. 7a, b, respectively). At a frequency of 0.1 Hz, neat PP shows storage and loss moduli around 0.25 and 35 Pa, respectively, whereas the nanocomposite with 3% of CNC_D exhibit higher values which are in the order of 8 and 131 Pa. On the other hand, the nanocomposites with 1% of CNC_D and 3% of CNC-Gr reveal equivalent storage and loss moduli which are approximately of 1.65 and 77 Pa, while the formulation with 1% of CNC-Gr presents obviously lower values. The nanocomposites moduli increase with the test frequency and at higher frequency values, the rheograms converge and intertwine. Correspondingly, Fig. 7c suggest that the PP/CNC-Co nanocomposites present higher complex viscosity compared to PP/CNC-Gr ones; indeed, it increases from 452 Pa s^{-1} for PP to 745 and 1141 Pa s^{-1} for the nanocomposites with 1 and 3% of CNC_D, respectively, against 426 and 722 Pa s^{-1}, for those with 1 and 3% of CNC-Gr. Such results testify that thanks to PP-g-MA, a highly interlocked and continuous system is made up of PP and CNC_D, owing to the connection of the nanoparticles to the matrix via the reaction of the CNC_D's hydroxyls and the MA groups of the compatibilizer. Nevertheless, the lower viscosity of PP/CNC-Gr gives evidence of a weak interfacial zone that is responsible, within the nanocomposite, for the discontinuity which induces a poor stress transfer, as concluded from the above results. Likewise, previous studies reported that when CNCs are dispersed homogeneously in a polymer matrix, an increase in both G′ and G″ is observed proportionally with the nanofiller content, thanks to the efficient stress transfer from the matrix to the nanoparticles [46, 47]. Additionally, cellulose nanocrystals were shown to lodge between the polymer's chains, thus affecting the matrix viscoelastic properties and enhancing the complex viscosity [48, 49].

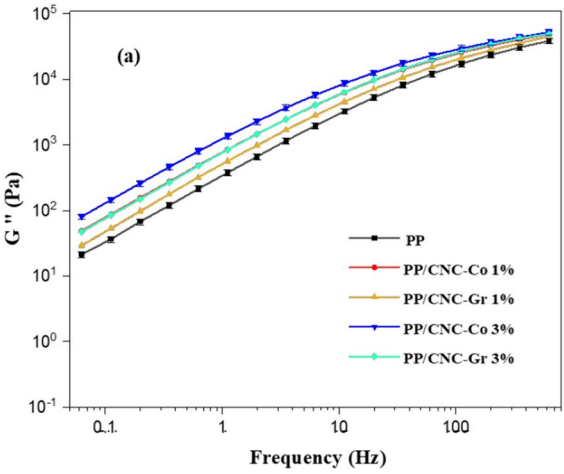
(a)
G '' (Pa)
Frequency (Hz)
PP
PP/CNC-Co 1%
PP/CNC-Gr 1%
PP/CNC-Co 3%
PP/CNC-Gr 3%

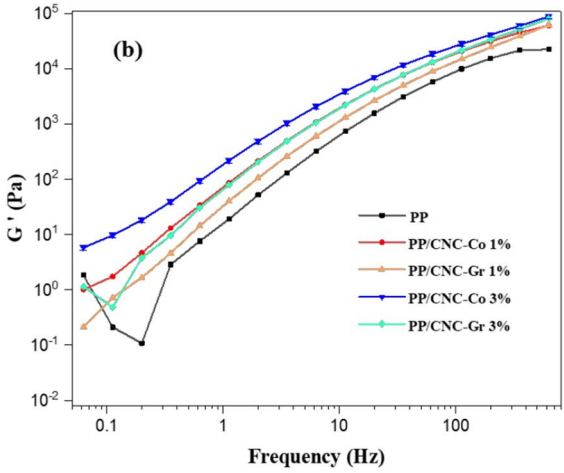
(b)
G ' (Pa)
Frequency (Hz)
PP
PP/CNC-Co 1%
PP/CNC-Gr 1%
PP/CNC-Co 3%
PP/CNC-Gr 3%

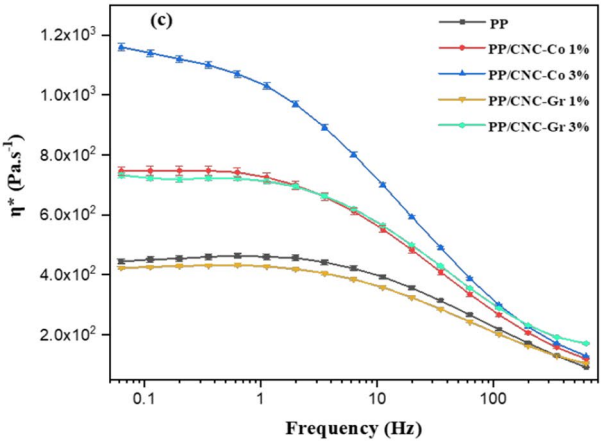
(c)
η* (Pa.s-1)
Frequency (Hz)
PP
PP/CNC-Co 1%
PP/CNC-Co 3%
PP/CNC-Gr 1%
PP/CNC-Gr 3%

Thermal stability

As it is widely recognized, one of the major drawbacks of the incorporation of cellulosic fibers within polymers is their premature decomposition, owing to their lower thermal stability, thus leaving residues which accelerate the matrix degradation [50]. Contrariwise, CNCs effect on polymers thermal stability has been subject to many controversial views in the literature. In this sense, it has been reported that CNC's incorporation in a polyhydroxybutyrate (PHB)/polycaprolactone (PCL) matrix leads to a decrease in thermal stability due to CNC's decomposition [51]. In opposition, Pinheiro et al. [34] attributed the higher thermal stability of poly (butylene adipate-co-terephthalate) (PBAT)/octadecyl isocyanate modified CNCs to the functionalization which leads to the reduction of sulfate groups on the CNC surface and the higher crystalline structure of the CNCs, as evinced by many other authors [52, 53]. Nevertheless, Fortunati et al. [30] pointed out that the addition of modified CNCs does not affect the degradation behavior of polymers.

Figure 8 represents the thermograms giving the TG and its derivative vs time (DTG) for PP and PP/CNC nanocomposites. Also, Table 3 reports temperatures corresponding to the degradation on-set (T_0) and end-set (Te), and the temperatures related to 5% ($T_{5\%}$) and 50% ($T_{50\%}$) of weight loss and degradation rate (V_d). A single degradation step is observed for neat PP, PP/CNC-Co and PP/CNC-Gr nanocomposites. Moreover, it is noticed that for 3 and 5% CNC_D's contents, both PP/CNC-Co and PP/CNC-Gr nanocomposites show higher thermal stability compared to PP matrix. Besides, it appears that PP/CNC-Co nanocomposites exhibit obvious improvement relatively to PP/CNC-Gr; T_0 increases from 400 °C for neat PP to 420 °C for both nanocomposites with 3 and 5% of CNC_D and to 414 °C for the formulation with 3% CNC-Gr but decreases to 373 °C for the nanocomposite filled with 5% of CNC-Gr. At the same time, $T_{5\%}$, $T_{50\%}$ and V_d increase by approximately 21 °C, 7 °C and 0.2 %/min, respectively, for the nanocomposites PP/CNC-Co. It is presumed that, initially, the interactions between CNC_Ds and the compatibilizer incite the wrapping of the unmodified nanoparticles by PP chains owing to PP-g-MA compatibilizer thus delaying their degradation process. Thereafter, when the degradation process is set up in the whole sample, an effective heat transfer ensued due to the intimate contact between the nanocomposite's components. Agarwal and al. [54] explained that the incorporation of PP-g-MA reduces the number of hydroxyl groups by the formation of ester linkage, thereby revealing greater thermal stability. These findings fit well the above discussed mechanical and morphological results which support the interfacial reaction with the compatibilizer and the embedding of the cellulose nanocrystals by PP. On the other hand, it appears also that the PP fraction used for MA grafting on CNC_Ds could have enrobed the nanocrystals by a thin protective layer of polymer that might preserve the CNC_Ds from a premature decomposition, as it is witnessed by the higher T_0, $T_{5\%}$, $T_{50\%}$ and lower V_d values.

All characterization results are shown in Table 4 for a better comparison.

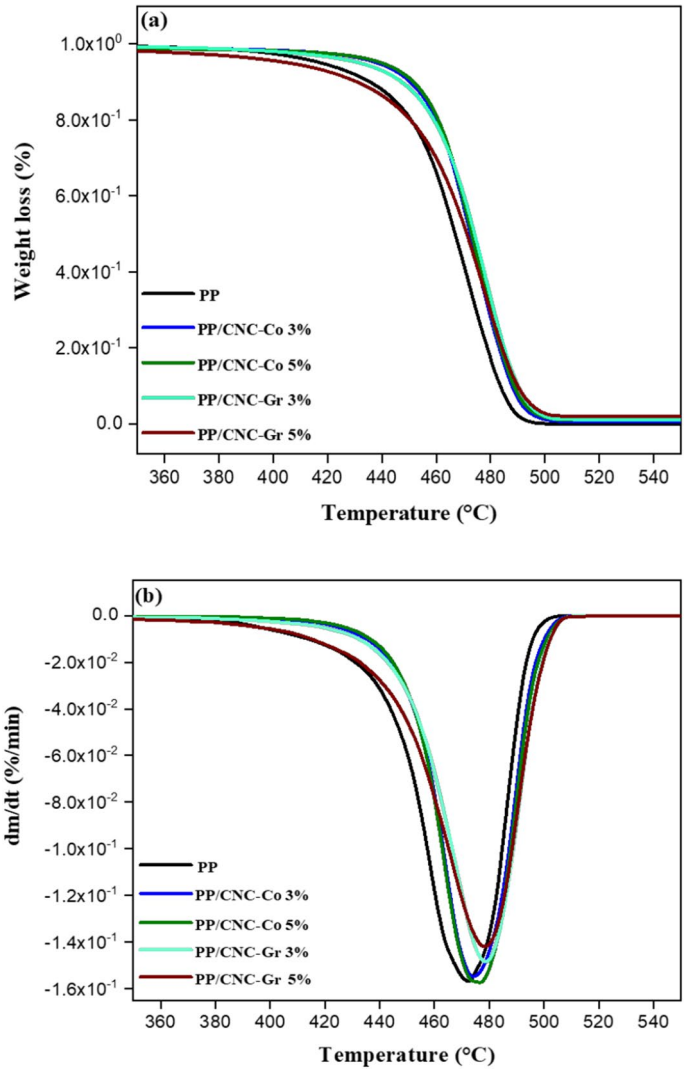

Fig. 8 TG (**a**) and DTG (**b**) thermograms of PP/CNC-Co and PP/CNC-Gr nanocomposites

Table 3 TGA results for PP/CNC-Co and PP/CNC-Gr nanocomposites

Parameters	T_0 (°C)	$T_{5\%}$ (°C)	$T_{50\%}$ (°C)	T_e(°C)	V_d (%/min^{-1})
PP	400	417	465	490	0.50
PP/CNC-Co 3%	420	438	472	496	0.58
PP/CNC-Co 5%	420	438	472	496	0.62
PP/CNC-Gr 3%	414	431	473	498	0.50
PP/CNC-Gr 5%	373	405	469	498	0.44

Table 4 Comparative summary of improved properties for PP/CNC_D

Characterization		Results		
		PP	PP/CNC-Co (3%)	PP/CNC-Gr (3%)
Rheological properties	Storage modulus (Pa)	0.25	8	131
	Loss modulus (Pa)	35	1.65	77
	Complex viscosity ($Pa.s^{-1}$)	452	1141	722
Impact strength (kJ/m^2)		22	17	14
Tensile properties	Tensile strength (MPa)	24	33	25
	Young modulus (MPa)	1945	2491	1957
	Elongation at break (%)	3	5	3
Thermal stability		<	>	

Conclusions

In the present paper, cellulose nanocrystals extracted from El Diss (CNC_D) fibers were incorporated into polypropylene (PP) matrix to prepare a novel nanocomposite with improved performances. For this achievement, CNC_D have been incorporated via two masterbatches, one based on in situ chemical grafting of PP and CNC_D with maleic anhydride and the second formed from unmodified CNC_D compatibilized with the matrix using a commercial PP-g-MA.

Thermo-mechanical, morphological and rheological results brought sufficient details to support the occurrence of interactions between the materials components for both types of formulations.

PP/CNC-Co nanocomposites are the most promising ones. These nanocomposites showed enhanced impact strength and tensile properties relatively to PP/CNC-Gr ones, because of the good adhesion resulting from coupling the CNC_Ds and the matrix via the interfacial reaction between MA and hydroxyl groups. Subsequently, PP/CNC-Co exhibited improved thermal stability due to the better inclusion of the CNC_D into the polymer, thus increasing obviously the nanocomposites complex viscosity. Conversely, it is thought that the grafting of MA on CNC_D and their wrapping by PP is not complete. So, the hydrophilic character is still pronounced and does not allow an optimal dispersion into the hydrophobic PP, resulting in lower tensile and impact properties, compared to PP and PP/CNC-Co nanocomposites. Nevertheless, the partial coverage of CNC_D by PP contributes in improving the nanocomposites thermal stability and increasing the complex viscosity.

Finally, regarding the achieved results, the dispersion of cellulose nanocrystals in polymeric matrices through the used masterbatch method seems to be a simple and promising effective route, from the practical point of view, since it may offer, also in a large scale, the opportunity to attain optimal CNC's dispersion into polymeric matrices.

Author contributions Conceptualization was done by MG and AM; Investigation was done by LB; Methodology was done by LB, TA, YA, HC, IA and MK; Supervision was done by MG, AM, YG, MC and

SD; Validation was done by TA, YA, HC, IA, MK, MG, AM and YG; Visualization was done by LB; Writing—original draft were done by LB; Writing—review & editing were done by MC and SD.

Funding Open access funding provided by Università degli Studi di Padova within the CRUI-CARE Agreement.

Declarations

Conflict of interest The authors declare no conflict of interest.

References

1. Kyrikou I, Briassoulis D (2007) Biodegradation of agricultural plastic films: a critical review. J Polym Environ 15:125–150
2. Thompson L, Azadmanjiri J, Nikzad M, Sbarski I, Wang J, Yu A (2019) Cellulose nanocrystals: production, functional-ization and advanced applications. Rev Adv Mater Sci 58:1–16
3. Prathapan R, Tabor RF, Garnier G, Hu J (2020) The recent progress of cellulose nanocrystals alignment and its applications. ACS Appl Bio Mater 3:1828–1844
4. Pandey JK, Ahn SH, Lee CS, Mohanty AK, Misra M (2010) Recent advances in the application of natural fiber based composites. Macromol Mater Eng 295:975–989
5. Dufresne A (2017) Cellulose nanomaterial reinforced polymer nanocomposites. Curr Opin Colloid Interface Sci 29:1–8
6. Puitel AC, Tofanica BM, Gavrilescu D, Petrea PV (2011) Environmentally sound vegetal fiber–polymer matrix composites. Cellul Chem Technol 45:265–274
7. Shojaeiarani J, Bajwa DS, Chanda S (2021) Cellulose nanocrystal based composites: a review. Compos C: Open Access 5:100164–100176
8. Mokhena TC, John MJ (2020) Cellulose nanomaterials: new generation materials for solving global issues. Cellulose 27:1149–1194
9. Favier V, Chanzy H, Cavaille JY (1995) Polymer nanocomposites reinforced by cellulose whiskers. Macromolecules 28:6365–6367
10. Islam MS, Chen L, Sisler J, Tam KC (2018) Cellulose nanocrystal (CNC)–inorganic hybrid systems: synthesis, properties and applications. J Mater Chem B 6:864–883
11. Purkait BS, Ray D, Sengupta S, Kar T, Mohanty A, Misra M (2011) Isolation of cellulose nanoparticles from sesame husk. Ind Eng Chem Res 50:871–876
12. Peng BL, Dhar N, Liu HL, Tam K (2011) Chemistry and applications of nanocrystalline cellulose and its derivatives: a nanotechnology perspective. Can J Chem Eng 89:1191–1206
13. Wang J, Liu X, Jin T, He H, Liu L (2019) Preparation of nanocellulose and its potential in reinforced composites: a review. J Biomater Sci Polym Ed 30:1–28
14. Hon-Meng S, Lee Tin B, Soo-Tueen T, Tee TT, Rahmat AR (2017) Review of nanocellulose polymer composite char-acteristics and challenges. Polym Plast Technol Eng 56:687–731
15. Panel Y, Dharmesh H, Chinmay H, Debasree K, Saurabh T, Shyam T, Jitendra N, Aniruddha C (2021) Cellulose bi-onanocomposites for sustainable planet and people: A global snapshot of preparation, properties, and applications. Carbohydr Polym Technol Appl 2:100065–100089
16. Azizi SMAS, Alloin F, Sanchez JY, El Kissi N, Dufresne A (2004) Preparation of cellulose whiskers reinforced nano-composites from an organic medium suspension. Macromolecules 37:1386–1393

17. Zhang W, Zhang Y, Cao J, Jiang W (2020) Improving the performance of edible food packaging films by using nanocellulose as an additive. Int J Biol Macromol 166:288–296
18. Feldman D (2015) Cellulose nanocomposites. J Macromol Sci 52:322–329
19. González-López ME, Robledo-Ortíz JR, Manríquez-González R, Silva-Guzmán JA, Pérez-Fonseca AA (2018) Polylactic acid functionalization with maleic anhydride and its use as coupling agent in natural fiber biocomposites: a review. Compos Interfaces 25:1–24
20. Geng S, Haque MM, Oksman K (2016) Crosslinked poly (vinyl acetate) (PVAc) reinforced with cellulose nanocrystals (CNC): structure and mechanical properties. Compos Sci Technol 126:35–42
21. Ng HM, Sin LT, Bee ST, Tee TT, Rahmat AR (2016) Review of nanocellulose polymer composite characteristics and challenges. Polym Plast Technol Eng 56:687–731
22. Benchikh L, Merzouki A, Grohens Y, Guessoum M, Pillin I (2020) Characterization of cellulose nanocrystals extracted from El Diss and El Retma local plants and their dispersion in poly (vinyl alcohol-co-ethylene) matrix in the presence of borax. Polym Polym Compos 29:218–230
23. Seta FT, An X, Liu L, Zhang H, Yang J, Zhang W, Liu H (2020) Preparation and characterization of high yield cellulose nanocrystals (CNC) derived from ball mill pretreatment and maleic acid hydrolysis. Carbohydr Polym 234:115942–115952
24. Samyn P (2022) Confined crystallization of thin plasma-polymerized nanocomposite films with maleic anhydride and cellulose nanocrystals under hydrolysis. Molecules 27:5683–5701
25. An S, Ma X (2017) Properties and structure of poly (3-hydroxybutyrate-co-4- hydroxybutyrate)/ wood fiber biodegradable composites modified with maleic anhydride. Ind Crops Prod 109:882–888
26. Girouard N, Schueneman GT, Shofner ML, Meredith JC (2015) Exploiting colloidal interfaces to increase dispersion, per-formance, and pot-life in cellulose nanocrystal/waterborne epoxy composites. Polymers 68:111–121
27. Kassab Z, Aziz F, Hannache H, Youcef HB, El Achaby M (2018) Improved mechanical properties of k-carrageenan-based nanocomposite films reinforced with cellulose nanocrystals. Int J Biol Macromol 123:1248–1256
28. Garcia-Garcia D, Lopez-Martinez J, Balart R, Strömberg E, Moriana R (2018) Reinforcing capability of cellulose nanocrys-tals obtained from pine cones in a biodegradable poly (3-hydroxybutyrate)/ poly (ε-caprolactone) (PHB/PCL) thermo-plastic blend. Eur Polym J 104:10–18
29. George J, Siddaramaiah (2012) High performance edible nanocomposite films containing bacterial cellulose nanocrystals. Carbohydr Polym 87:2031–2037
30. Fortunati E, Luzi F, Puglia D, Terenzi A, Vercellino M, Visai L, Kenny JM (2013) Ternary PVA nanocomposites con-taining cellulose nanocrystals from different sources and silver particles: part II. Carbohydr Polym 97:837–848
31. Haque MMU, Puglia D, Fortunati E, Pracella M (2017) Effect of reactive functionalization on properties and degradabil-ity of poly (lactic acid)/poly (vinyl acetate) nanocomposites with cellulose nanocrystals. React Funct Polym 110:1–9
32. Koohestani B, Darban AK, Mokhtari P, Yilmaz E, Darezereshki E (2018) Comparison of different natural fiber treatments: a literature review. Int J Environ Sci Technol 16:629–642
33. Gwon J, Cho H, Lee D, Choi D, Lee S, Wu Q, Lee S (2018) Physicochemical and mechanical properties of polypropylene-cellulose nanocrystal nanocomposites: effects of manufacturing process and chemical grafting. Bioresour 13:1619–1636
34. Pinheiro IF, Ferreira FV, Souza DHS, Gouveia RF, Lona LMF, Morales AR, Mei LHI (2017) Mechanical, rheological and degradation properties of PBAT nanocomposites reinforced by functionalized cellulose nanocrystals. Eur Polym J 97:356–365
35. Gunning MA, Geever LM, Killion JA, Lyons JG, Higginbotham CL (2013) Mechanical and biodegradation performance of short natural fibre polyhydroxybutyrate composites. Polym Test 32:1603–1611
36. Hammiche D, Boukerrou A, Djidjelli H, Djerrada A (2013) Effects of some PVC-grafted maleic anhydrides (PVC-g-MAs) on the morphology, and the mechanical and thermal properties of (alfa fiber)-reinforced PVC composites. J Vinyl Addit Technol 19:225–232
37. El Achaby M, Kassab Z, Barakat A, Aboulkas A (2018) Alfa fibers as viable sustainable source for cellulose nanocrystals extraction: application for improving the tensile properties of biopolymer nanocomposite films. Ind Crops Prod 112:499–510
38. Carrera AF (2017) Coupling agent usage in the preparation of cellulose nanofibril (CNF)and cellulose nanocrystal (CNC)-based nanocomposites. In: Kargarzadeh H, Ahmad I, Thomas S, Dufresne A (eds) Handbook of nanocellulose and cellulose nanocomposites, 1st edn. Wiley, New York, pp 334–365

39. Buffa JM, Mondragon G, Corcuera MA, Eceiza A, Mucci V, Aranguren MI (2018) Physical and mechanical properties of a vegetable oil-based nanocomposite. Eur Polym J 98:116–124
40. Kabache F, Nekkaa S, Guessoum M (2022) Alkali and epoxy-silane surface modified pine cone flour reinforced polypro-pylene/poly (lactic acid) blend:viscoelastic and morphological characterization. J Adhes Sci Technol 36:1017–1040
41. Benhamou K, Kaddami H, Magnin A, Dufresne A, Ahmad A (2015) Bio-based polyurethane reinforced with cellulose nanofibers: a comprehensive investigation on the effect of interface. Carbohydr Polym 122:202–211
42. Trinh BM, Mekonnen T (2018) Hydrophobic esterification of cellulose nanocrystals for epoxy reinforcement. Polymers 155:64–74
43. Abraham E, Kam D, Nevo Y, Slattegard R, Rivkin A, Lapidot S, Shoseyov O (2016) Highly modified cellulose nano-crystals and formation of epoxy-nanocrystalline cellulose (CNC) nanocomposites. ACS Appl Mater Interfaces 8:28086–28095
44. Benchikh L, Aitferhat Y, Kebaili M, Chorfi H, Abacha I, Guessoum M, Merzougui A, Benia HM, Grohens Y (2023) Acetylation of cellulose nanocrystals extracted from cotton for drilling fluid application: structural and thermal characterization. Int J Nanosci 22:2350036
45. Agarwal J, Mohanty S, Nayak SK (2020) Valorization of pineapple peel waste and sisal fiber: study of cellulose nanocrystals on polypropylene nanocomposites. J Appl Polym Sci 137:1–19
46. Mariano M, El Kissi N, Dufresne A (2016) Structural reorganization of CNC ininjectionmolded CNC/PBAT materials under thermal annealing. Langmuir 32:10093–10103
47. Zhang X, Ma P, Zhang Y (2016) Structure and properties of surface-acetylated cellulose nanocrystal/poly (butylene adipate-co-terephthalate) composites. Polym Bull 73:2073–2085
48. Durmus A, Kasgoz A, Macosko CW (2007) Linear low density polyethylene (LLDPE)/clay nanocomposites. Part I: structural characterization and quantifying clay dispersion by melt rheology. Polymer (Guildf) 48:4492–4502
49. Benchikh L, Merzouki A, Grohens Y, Pellin I (2019) Extruded poly (ethylene–co–vinyl alcohol) composite films reinforced with cellulosic fibers isolated from two local abundonates plants. J Fundam Appl Sci 12:49–72
50. Rahem Z, Mayouf I, Guessoum M, Delaite C, Douibi A, Lallam A (2019) Compatibilization of biocomposites based on sponge gourd natural fiber reinforced poly(lactic acid). Polym Compos 40:4489–4499
51. Yu H, Qin Z, Zhou Z (2011) Cellulose nanocrystals as green fillers to improve crystallization and hydrophilic property of poly (3-hydroxybutyrate-co-3- hydroxyvalerate). Prog Nat Sci 21:478–484
52. Liu C, Li B, Du H, Lv D, Zhang Y, Yu G, Mu X, Peng H (2016) Properties of nanocellulose isolated from corncob residue using sulfuric acid, formic acid, oxidative and mechanical methods. Carbohydr Polym 151:716–724
53. Timhadjelt L, Serier A, Belgacem MN, Bras J (2015) Elaboration of cellulose based nanobiocomposite: effect of cellulose nanocrystals surface treatment and interface "melting." Ind Crops Prod 72:7–15
54. Agarwal J, Mohanty S, Nayak SK (2021) Influence of cellulose nanocrystal/sisal fiber on the mechanical, thermal, and morphological performance of polypropylene hybrid composites. Polym Bull 78:1609–1635

Authors and Affiliations

Lilia Benchikh[1] · Tahar Aouissi[2] · Yazid Aitferhat[3] · Hichem Chorfi[3] · Ilyes Abacha[3] · Maya Kebaili[3] · Melia Guessoum[4] · Abdelhafid Merzouki[4] · Yves Grohens[5] · Mauro Carraro[6,7] · Souad Djellali[4,8]

✉ Mauro Carraro
mauro.carraro@unipd.it

✉ Souad Djellali
souad.djellali@univ-setif.dz

Lilia Benchikh
lilia.benchikh@gmail.com

Tahar Aouissi
aouissi.tahar@yahoo.com

Yazid Aitferhat
aitferhatyazid@gmail.com

Hichem Chorfi
chorfihichemdoc19@gmail.com

Ilyes Abacha
Ilyesabacha@gmail.com

Maya Kebaili
kebailimaya@yahoo.fr

Melia Guessoum
guessoum_melia@yahoo.fr

Abdelhafid Merzouki
hafid_merzouki@yahoo.fr

Yves Grohens
yves.grohens@univ-ubs.fr

[1] Centre de Recherche en Technologies Agroalimentaires, Route de Targa Ouzemmour, Campus Universitaire, 06000 Bejaia, Algeria

[2] Laboratoire des Matériaux Polymériques Multiphasiques (LMPMP), Université Ferhat Abbas Sétif-1, 19000 Setif, Algeria

[3] Centre de recherche en mécanique, Campus ChaabErssas, Université les frères Mentouri 1, Constantine, Algeria

[4] Laboratoire de Physico-Chimie des Hauts Polymères, Département de Génie des Procédés, Faculté de Technologie, Université Ferhat Abbas Sétif 1, Setif, Algeria

[5] Institut de Recherche Dupuy de Lôme, UMR CNRS 6027, Université de Bretagne Sud, Lorient, France

[6] Department of Chemical Sciences, University of Padova, Via Marzolo 1, 35131 Padua, Italy

[7] Institute on Membrane Technology (ITM-CNR), UoS of Padova, Via Marzolo 1, 35131 Padua, Italy

[8] Department of Chemistry, Faculty of Sciences, University Ferhat Abbas Setif-1, 19000 Setif, Algeria